

## **BANDWIDTH ENHANCEMENT FOR SPLIT CYLINDRICAL DIELECTRIC RESONATOR ANTENNAS**

**A. A. Kishk and A. W. Glisson**

Department of Electrical Engineering  
The University of Mississippi, University, MS 38677, USA

**G. P. Junker**

501 W. Mariposa Ave., El Segundo, CA 90245, USA

**Abstract**—A numerical study of split cylindrical dielectric resonator antennas on a conducting ground plane excited by a coaxial probe is presented. The numerical solution is based on the method of moments for a body of revolution coupled to a wire. We consider in this study bandwidth enhancement for dielectric resonators excited in the  $HEM_{11}$  and  $HEM_{12}$  modes for the split dielectric cylinder. A wideband performance of about 35% has been achieved for the antenna and experimental measurements have verified this finding.

### **1 Introduction**

### **2 Ideal Performance**

### **3 Numerical Results**

### **4 Dual-band Antennas**

### **5 Summary**

### **Acknowledgment**

### **References**

## **1. INTRODUCTION**

Dielectric resonators are made of high dielectric constant materials. They have been used efficiently as microwave components in the design

of filters because of their high quality factor. Therefore, many engineers have doubted their suitability for use as a radiator, thinking that they would not be efficient radiators and that they would have a very small radiation bandwidth. It has, however, been shown that some modes have a small radiation  $Q$ -factor [1]. The radiation efficiency has also been measured for the  $\text{HEM}_{11\delta}$  mode of the cylindrical dielectric resonator with  $\epsilon_r = 38$  and was found to be better than 98% [2]. Interest has continued to increase in dielectric resonator antennas (DRA's) [3] due to their small size, efficiency, and potential ability to perform multiple antenna tasks via simple mode coupling mechanisms. More attention and study needs to be given to this antenna to obtain a better understanding of its performance characteristics. Accurate analysis of the DRA must be performed numerically and is somewhat difficult. Such analyses, however, help in the physical understanding for the performance of the antenna and in determining optimal usage of the antenna. Many studies have concentrated on the cylindrical DRA structures [4], for which the TM and quasi-TM modes may be excited by having the dielectric disk situated on a ground plane [5]. Little attention has been given to cylindrical DRA structures excited in the TE and quasi-TE modes, however, because these modes cannot be excited when the circular base of a cylindrical DRA is placed on a ground plane.

In this paper we briefly discuss some of the characteristics of the DRA's related to the  $\text{HEM}_{11\delta}$  and the  $\text{HEM}_{12\delta}$  modes compared to the more commonly studied  $\text{TM}_{01\delta}$  mode and the  $\text{TE}_{01\delta}$  mode. Some basics regarding their excitation mechanism are described, and empirical expressions are given to compute accurately the resonant frequency and the radiation  $Q$ -factor for the ideal case of an isolated, source-free DRA. To permit excitation of the  $\text{HEM}_{12\delta}$  mode for a resonator situated on a ground plane, a split cylindrical DRA such as shown in Fig. 1 is considered. The  $\text{HEM}_{11\delta}$  mode can also be excited in this configuration. Results are presented showing a broadband performance of the DRA excited in single mode operation, which reaches about 35%. Also, in some cases it is possible to have a dual band performance with the proper excitation of the DRA.

## 2. IDEAL PERFORMANCE

To easily design a DRA for a particular use, one must have a reasonable idea of the resonant frequency,  $Q$ -factor, and mode of operation for various geometrical parameters associated with the DRA. The resonant frequency and the radiation  $Q$ -factor for a particular configuration may be computed numerically through a search for the natural resonant

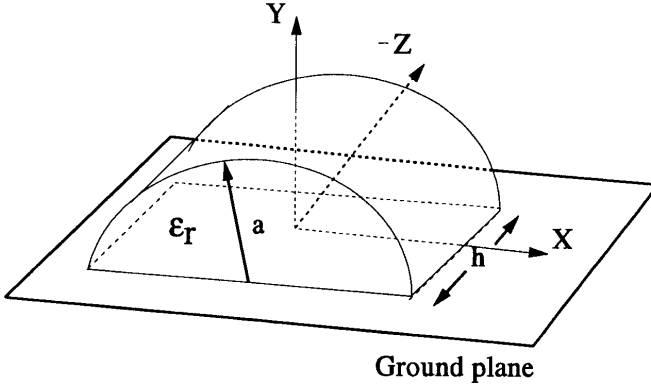


**Figure 1.** Geometry of the split cylindrical DRA.

frequencies (for a source free system) in the complex frequency plane as described in [6]. Once a natural frequency has been found, the mode associated with that natural frequency can be identified from its field distribution. Knowledge of the field distribution is also useful in determining an appropriate feed mechanism for the DRA.

For design purposes, however, this time consuming process would need to be repeated many times for different parameters until appropriate characteristics are achieved. It is desirable to have relatively accurate approximate methods to determine some of these characteristics quickly. Thus, we have computed the resonant frequencies and the radiation  $Q$ -factors for the first four modes, i.e., the  $TM_{01\delta}$ ,  $TE_{01\delta}$ ,  $HEM_{11\delta}$  and the  $HEM_{12\delta}$  modes, for a cylindrical DRA as a function of different  $a/h$  (radius to height) ratios and for dielectric constants of 10, 22, and 38. Curve-fit equations are then obtained for the resonant frequencies and the  $Q$ -factors of these modes in terms of these parameters as

$$k_0 a = 2.920415 \epsilon_r^{-0.465421} \times \left\{ 0.690841 + 0.319075 \left( \frac{a}{h} \right) - 0.035494 \left( \frac{a}{h} \right)^2 \right\} \quad (1)$$

and

$$Q = 0.012356 \epsilon_r^{1.207086} \times \left\{ 5.2696 \left( \frac{a}{h} \right) + 106.18807 \left( \frac{a}{h} \right)^{0.624875} e^{-1.027195 \left( \frac{a}{h} \right)} \right\} \quad (2)$$

for the  $TE_{01\delta}$  mode,

$$k_0 a = 2.932566 \epsilon_r^{-0.467715} \left\{ 1 - \left[ 0.075 - 0.05 \left( \frac{a}{h} \right) \right] \left[ \frac{\epsilon_r - 10}{28} \right] \right\} \\ \times \left\{ 1.047542 + 0.377422 \left( \frac{a}{h} \right) - 0.07112 \left( \frac{a}{h} \right)^2 \right\} \quad (3)$$

and

$$Q = 0.008721 \epsilon_r^{0.888413} e^{0.0397475 \epsilon_r} \left\{ 1 - \left[ 0.3 - 0.2 \left( \frac{a}{h} \right) \right] \left[ \frac{38 - \epsilon_r}{28} \right] \right\} \\ \times \left\{ 9.498196 \left( \frac{a}{h} \right) + 2058.33 \left( \frac{a}{h} \right)^{4.322261} e^{-3.50099 \left( \frac{a}{h} \right)} \right\} \quad (4)$$

for the  $TM_{01\delta}$  mode,

$$k_0 a = 2.734956 \epsilon_r^{-0.436076} \\ \times \left\{ 0.54318 + 0.589025 \left( \frac{a}{h} \right) - 0.049591 \left( \frac{a}{h} \right)^2 \right\} \quad (5)$$

and

$$Q = 0.012604 \epsilon_r^{1.201971} \times \left\{ 2.134757 \left( \frac{a}{h} \right) \right. \\ \left. + 228.0429 \left( \frac{a}{h} \right) e^{-2.046468 \left( \frac{a}{h} \right) + 0.110953 \left( \frac{a}{h} \right)^2} \right\} \quad (6)$$

for the  $HEM_{11\delta}$  mode, and

$$k_0 a = 3.114093 \epsilon_r^{-0.494406} \left\{ 1.189612 \right. \\ \left. - \left( 0.041212 - 3.408916 e^{-2.624985 \left( \frac{a}{h} \right)} \right) \left( \frac{a}{h} \right) \right. \\ \left. + 1.548193 \log \left( \frac{a}{h} \right) \right\} \quad (7)$$

and

$$Q = \left( 0.369661 + 0.02334 \epsilon_r + 0.001051 \epsilon^2 \right) \\ \cdot \left\{ 1 - 0.3 \left( \frac{38 - \epsilon_r}{28} \right)^2 \left[ 2.92 - \left( \frac{a}{h} \right) \right]^{0.8} \right\} \\ \times \left\{ 41.29139 \left( \frac{a}{h} \right)^{-2} - 110.8862 \left( \frac{a}{h} \right)^{-1} + \left( \frac{a}{h} \right) \right. \\ \left. \cdot \left( 15.58616 + 334.2778 e^{-1.070847 \left( \frac{a}{h} \right) - 0.084812 \left( \frac{a}{h} \right)^2} \right) \right\} \quad (8)$$

for the  $\text{HEM}_{12\delta}$  mode.

The actual results for the resonant frequencies and Q factors obtained from the numerical search in the complex frequency plane and results computed using the above expressions are given in Figs. 2 to 5. In these figures the symbols represent the values obtained directly from the numerical search and the lines represent results predicted from the above expressions. It can be seen that the results predicted using the expressions agree reasonably well with the results obtained from the numerical search. It should be noted that the same scales have been used for the graphs for each of the different modes so that comparisons can be fairly easily made between the different modes.

From the figures it is clear that the rates of change in the resonant frequency of the  $\text{TE}_{01\delta}$  and  $\text{HEM}_{12\delta}$  modes with respect to  $a/h$  are lower than those for the modes  $\text{TM}_{01\delta}$  and  $\text{HEM}_{11\delta}$ . This provides an indication of the possibility of better wideband performance for the  $\text{TE}_{01\delta}$  and  $\text{HEM}_{12\delta}$  modes than for those of the  $\text{TM}_{01\delta}$  and  $\text{HEM}_{11\delta}$  type. To excite these modes properly, knowledge of the near field distribution for each mode permits one to choose the excitation mechanism appropriately. An electric current excitation can be chosen by using a probe oriented along the high density electric field lines or a magnetic current excitation can be chosen by using narrow slots in the ground plane oriented along the high density magnetic field lines [1]. The ideal far field patterns for the  $\text{HEM}_{11\delta}$  and  $\text{HEM}_{12\delta}$  modes are given in Figs. 6 and 7, respectively. In these and other radiation pattern plots that appear subsequently, the angular variation shown on the polar plots represents the standard spherical coordinate angles  $\theta$  for  $y$ - $z$  plane plots and  $\psi$  for  $x$ - $y$  plane plots. These far field radiation patterns are obtained based on the assumption that only the desired mode is radiating. Thus, they can be used as a reference for comparison with the actual radiation patterns that are obtained where more than one mode may be excited and contributing to the radiation patterns.

### 3. NUMERICAL RESULTS

Excitation of the  $\text{HEM}_{11\delta}$  mode for the split cylindrical dielectric resonator antenna of Fig. 1 will result in a broadside radiation pattern. This broadside radiation pattern is similar to the radiation pattern of a narrow slot in a ground plane. The  $\text{HEM}_{11\delta}$  mode can be excited by a monopole displaced along the  $z$ -axis from the position of  $z_f = 0$  (see Fig. 8). For the results shown here, we have restricted the orientation and position of the monopole to be along the  $y$ -direction and on the  $z$ -axis, where the DRA is the tallest, to allow for the largest possible variations of the monopole length as shown

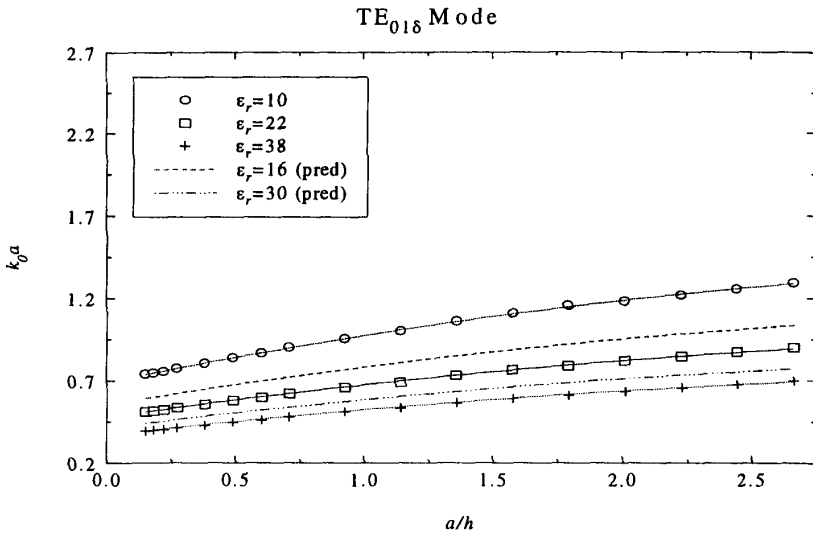


**Figure 2a.** Normalized resonant frequency for the TE<sub>01δ</sub> mode.

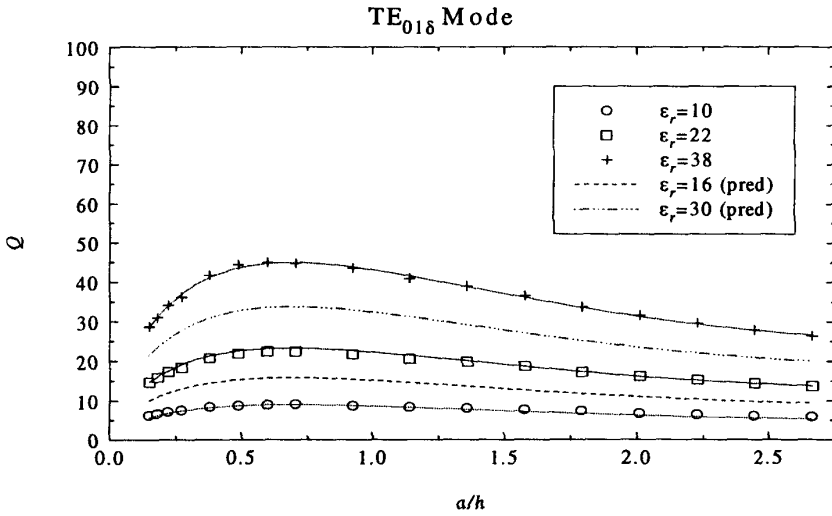


**Figure 2b.** Radiation  $Q$ -factor for the TE<sub>01δ</sub> mode.

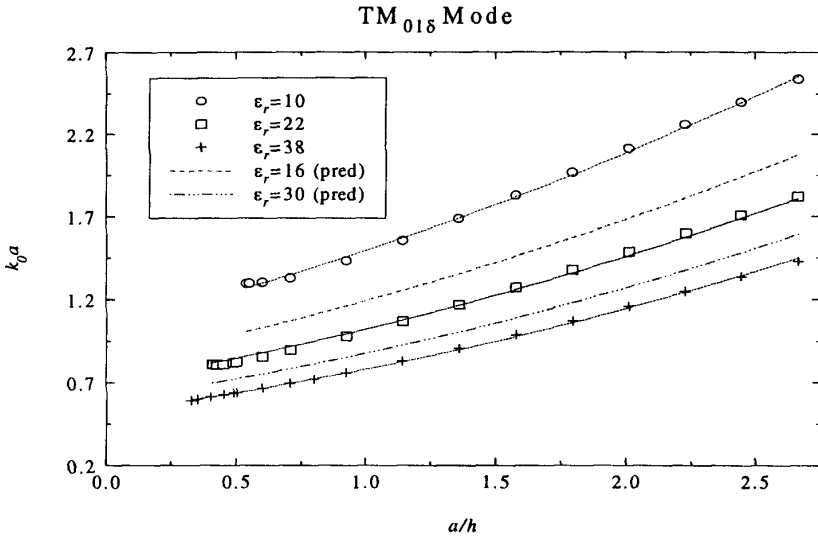


**Figure 3a.** Normalized resonant frequency for the TM<sub>01 $\delta$</sub>  mode.

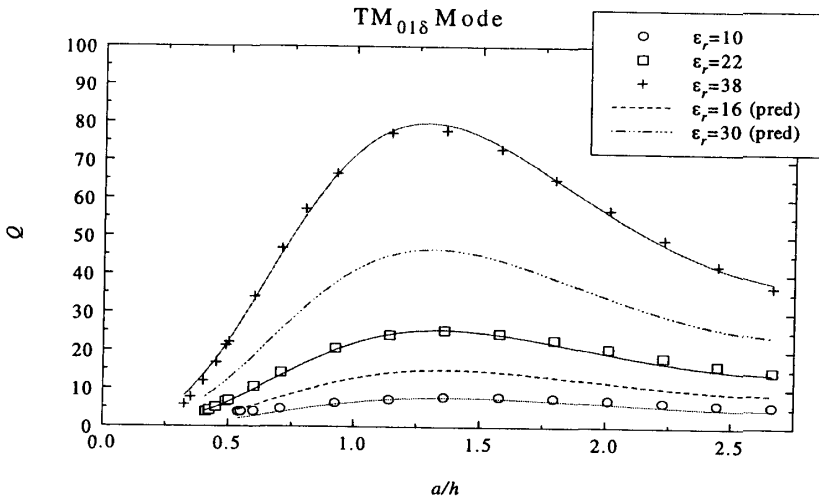


**Figure 3b.** Radiation  $Q$ -factor for the TM<sub>01 $\delta$</sub>  mode.

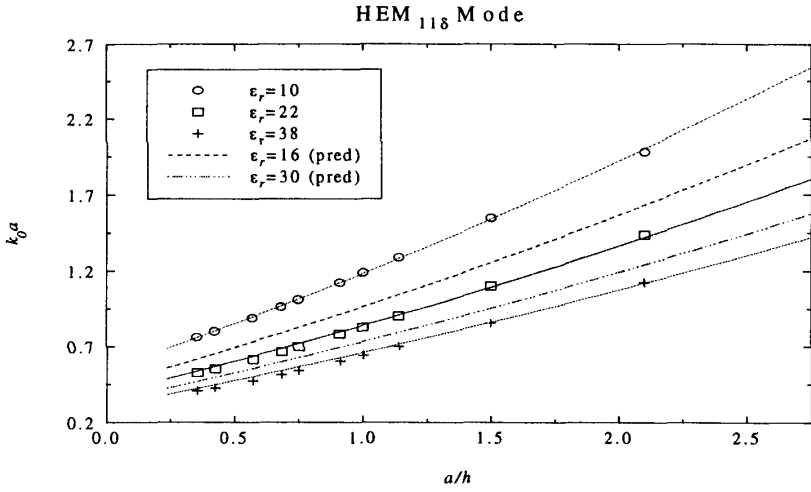


Figure 4a. Normalized resonant frequency for the HEM<sub>11δ</sub> mode.

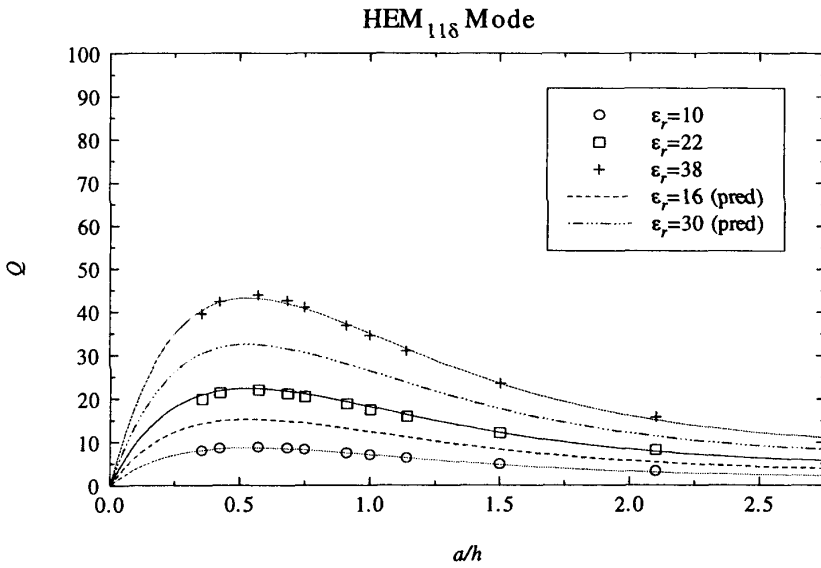


Figure 4b. Radiation  $Q$ -factor for the HEM<sub>11δ</sub> mode.

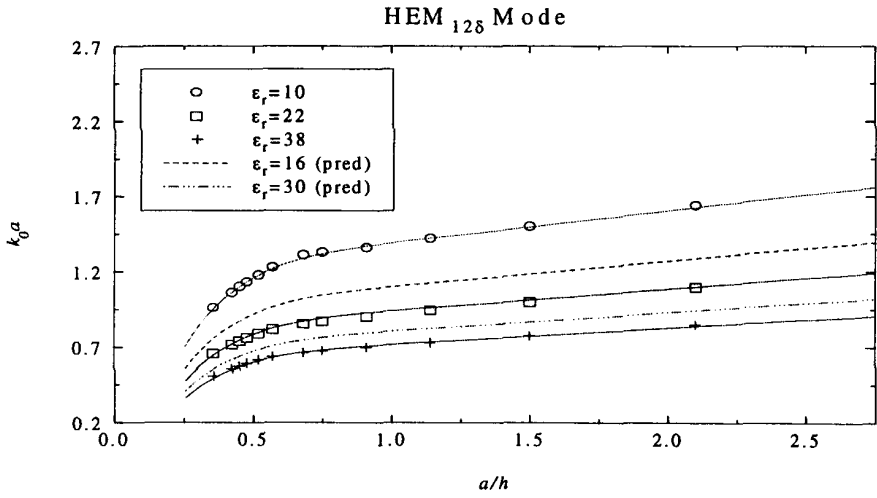


Figure 5a. Normalized resonant frequency for the  $HEM_{12\delta}$  mode.

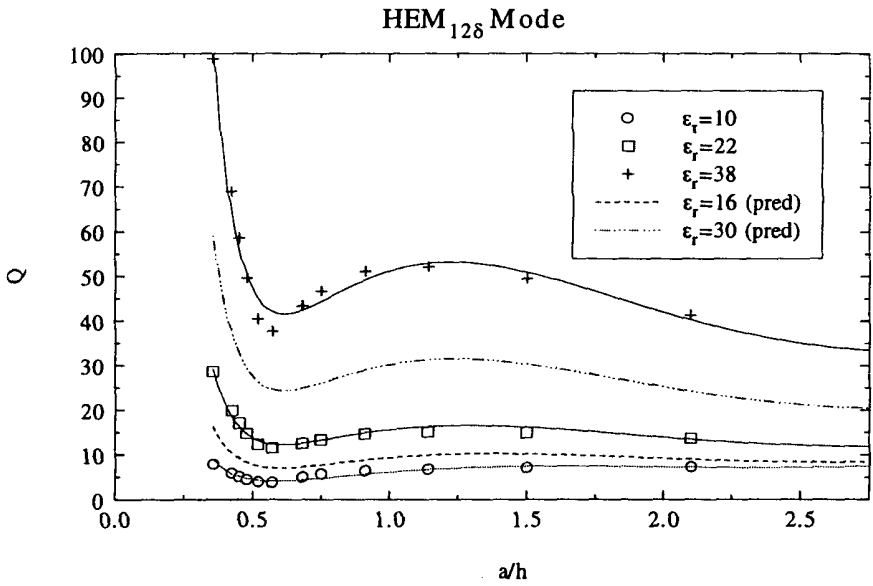


Figure 5b. Radiation  $Q$ -factor for the  $HEM_{12\delta}$  mode.

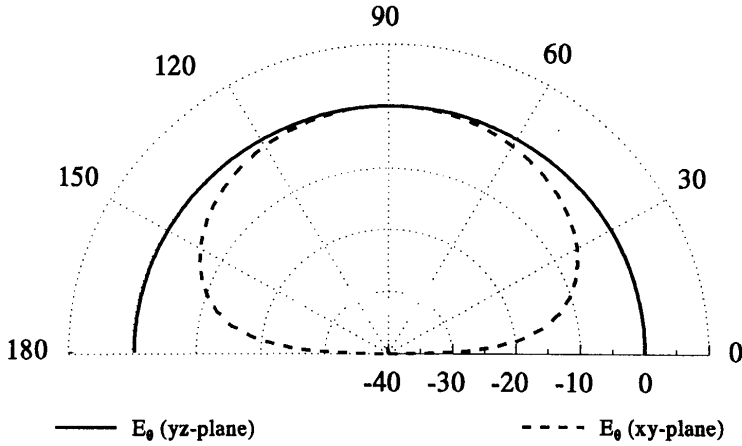


Figure 6. Radiation patterns of the  $\text{HEM}_{11\delta}$  mode.

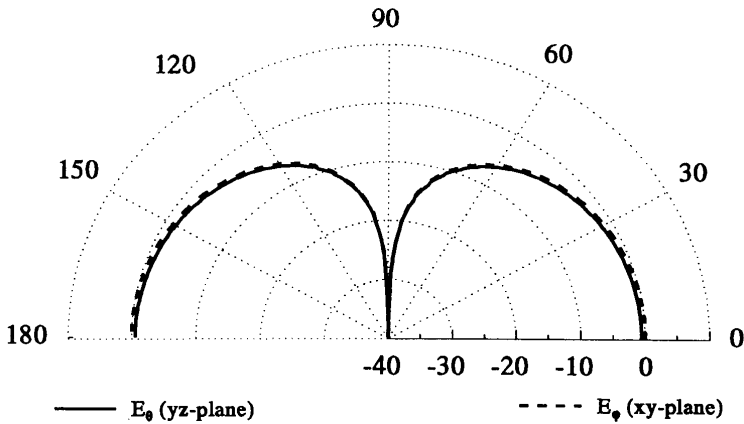
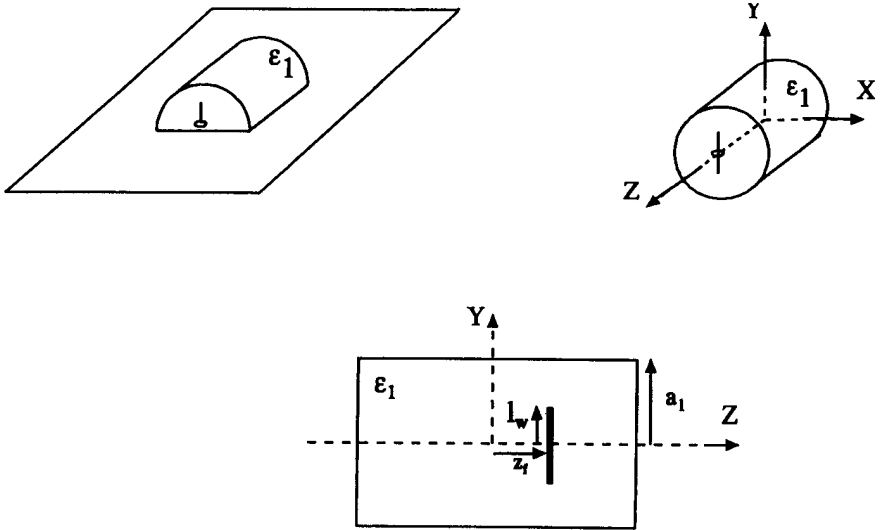
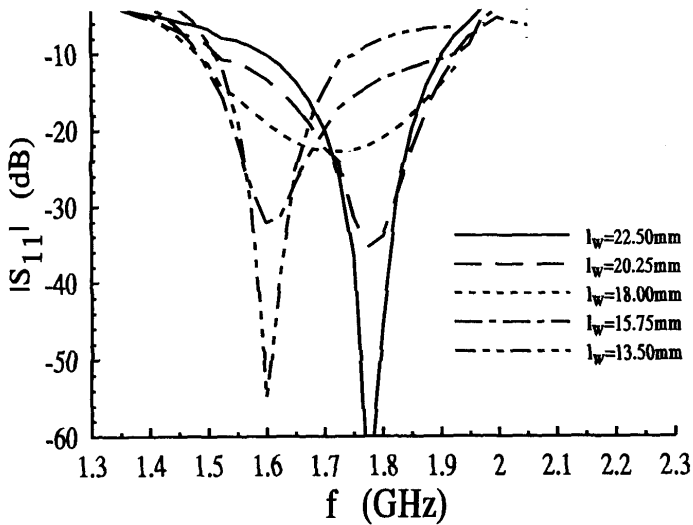


Figure 7. Radiation patterns of the  $\text{HEM}_{12\delta}$  mode.

in Fig. 8. Fig. 9 shows the return loss of the split resonator with  $a_1 = 2.25$  cm,  $h = 3.9$  cm,  $a_w = 0.0118$  cm,  $z_f = 15.8$  mm,  $\epsilon_r = 12$ , and with different wire lengths. Changing the wire length changes the return loss and shows that an optimum length of  $\ell_w = 18$  mm produces a bandwidth of about 22% ( $-10$  dB return loss bandwidth). Samples of the radiation patterns are computed at different frequencies as shown in Fig. 10. The radiation patterns show that the  $\text{HEM}_{11\delta}$  mode is excited efficiently within this band, as the radiations patterns are very



**Figure 8.** Geometry for the split DRA with vertical dipole located on the  $z$ -axis: 3-D and cross-section views.



**Figure 9.** Return loss versus frequency with  $z_f = 15.8$  mm.

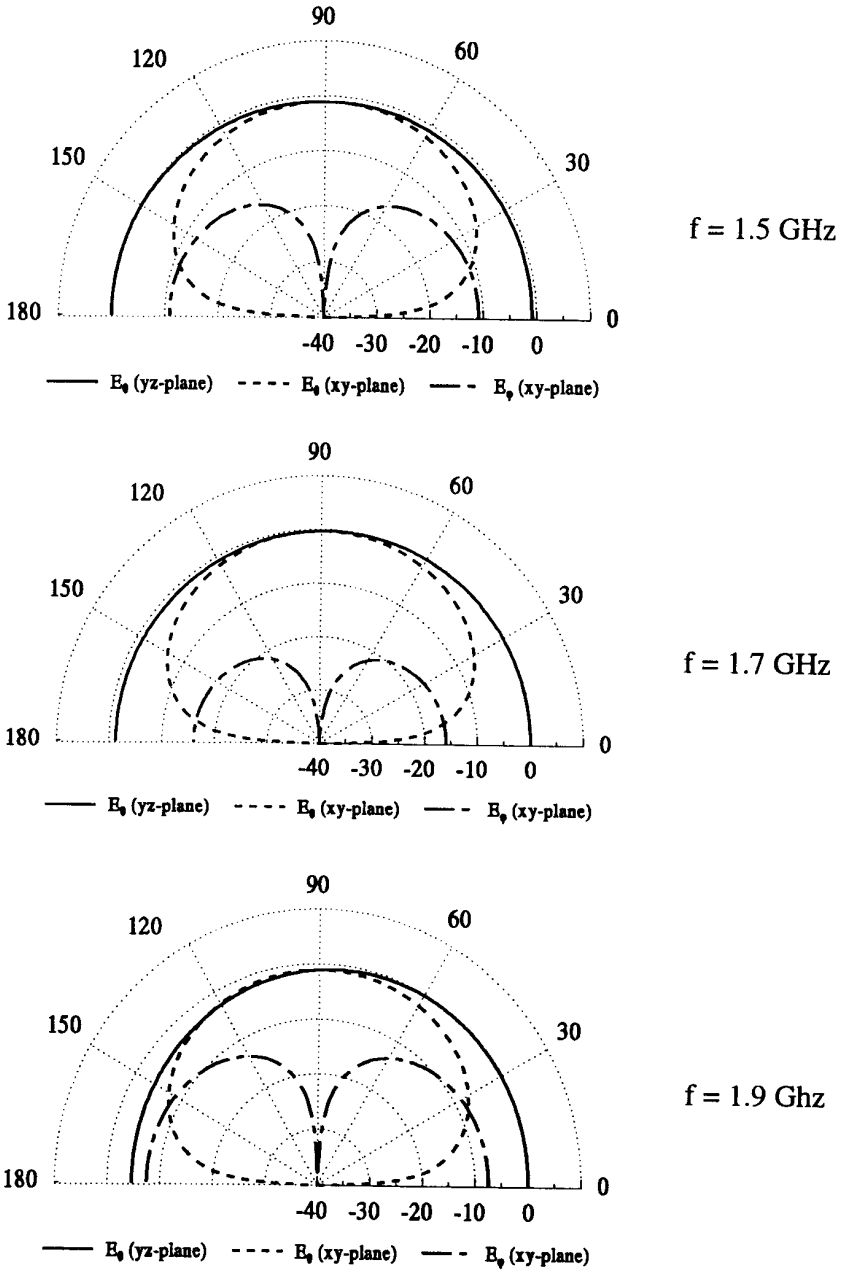
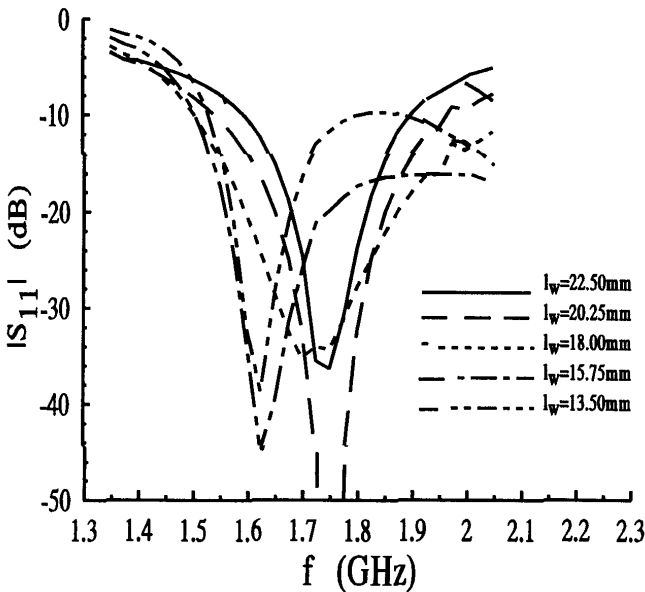


Figure 10. Radiation patterns with  $z_f = 15.8$  mm and  $\ell_w = 18$  mm.

similar over the frequency range from 1.5 GHz to 1.9 GHz.

When the excitation monopole is located at  $z_f = 11.85$  mm, i.e., closer to the center of the DRA, the bandwidth seems to be even wider than before, but a different monopole length ( $\ell_w = 15.75$  mm) is required as shown in Fig. 11. However, one observes in Fig. 12 that for this case the radiation pattern at  $f = 1.9$  GHz has deteriorated to be significantly different from that of the  $\text{HEM}_{11\delta}$  mode because other modes are being more strongly excited and have started to contribute more to the radiation pattern. When the monopole is placed even closer to the DRA center with  $z_f = 3.95$  mm, the matching bandwidth does not change much, as shown in Fig. 13, but the radiation patterns deteriorate even further at  $f = 1.7$  GHz and  $f = 1.9$  GHz as shown in Fig. 14. When the monopole is located at the DRA center with  $z_f = 0.0$  a very wide matching bandwidth is obtained as shown in Fig. 15. This bandwidth is about 35%. From the radiation patterns in Fig. 16, however, we can see that the radiating mode between the frequency range of 1.7 GHz to 2.3 GHz in this case is the  $\text{HEM}_{12\delta}$  mode rather than the  $\text{HEM}_{11\delta}$  mode.



**Figure 11.** Return loss versus frequency with  $z_f = 11.85$  mm.

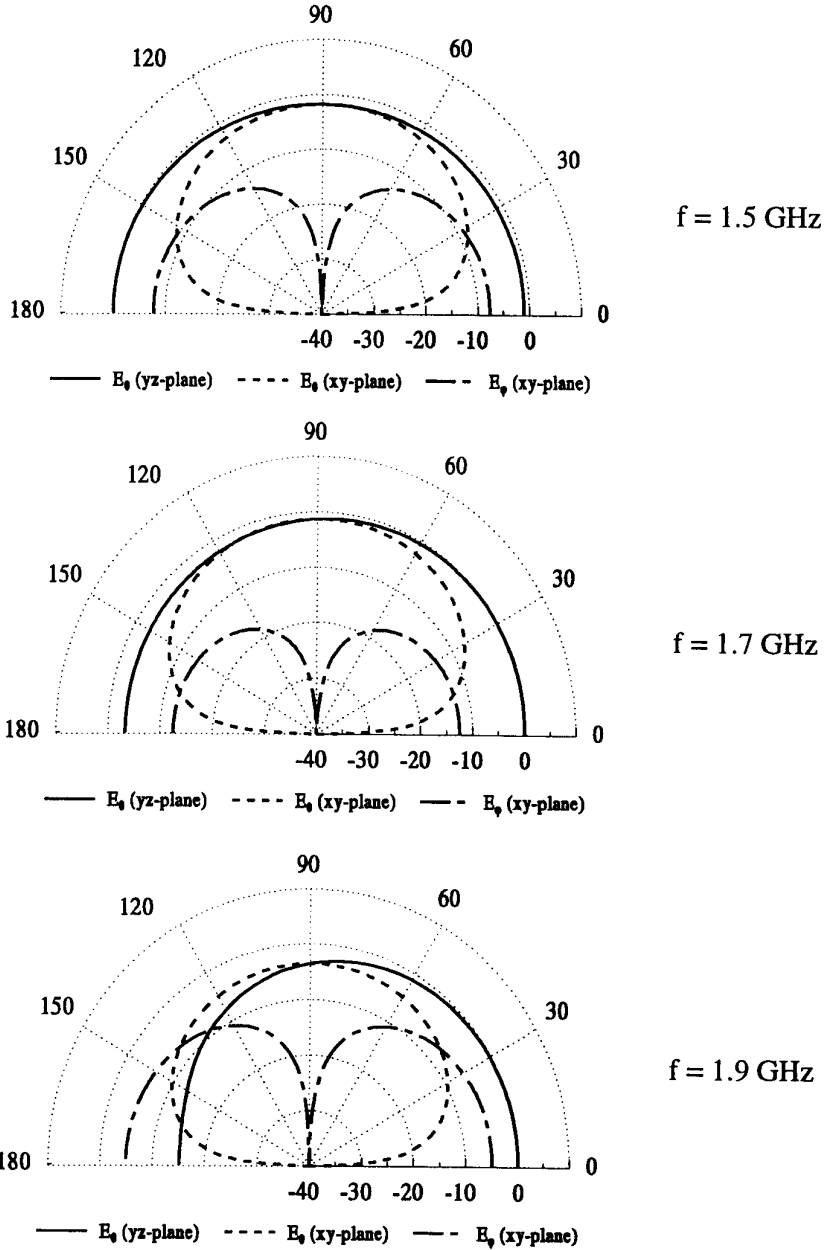


**Figure 12.** Radiation patterns with  $z_f = 11.85$  mm and  $\ell_w = 15.75$  mm.

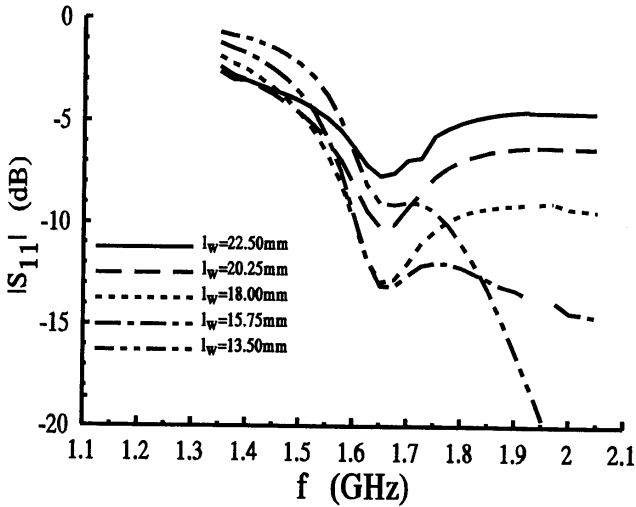
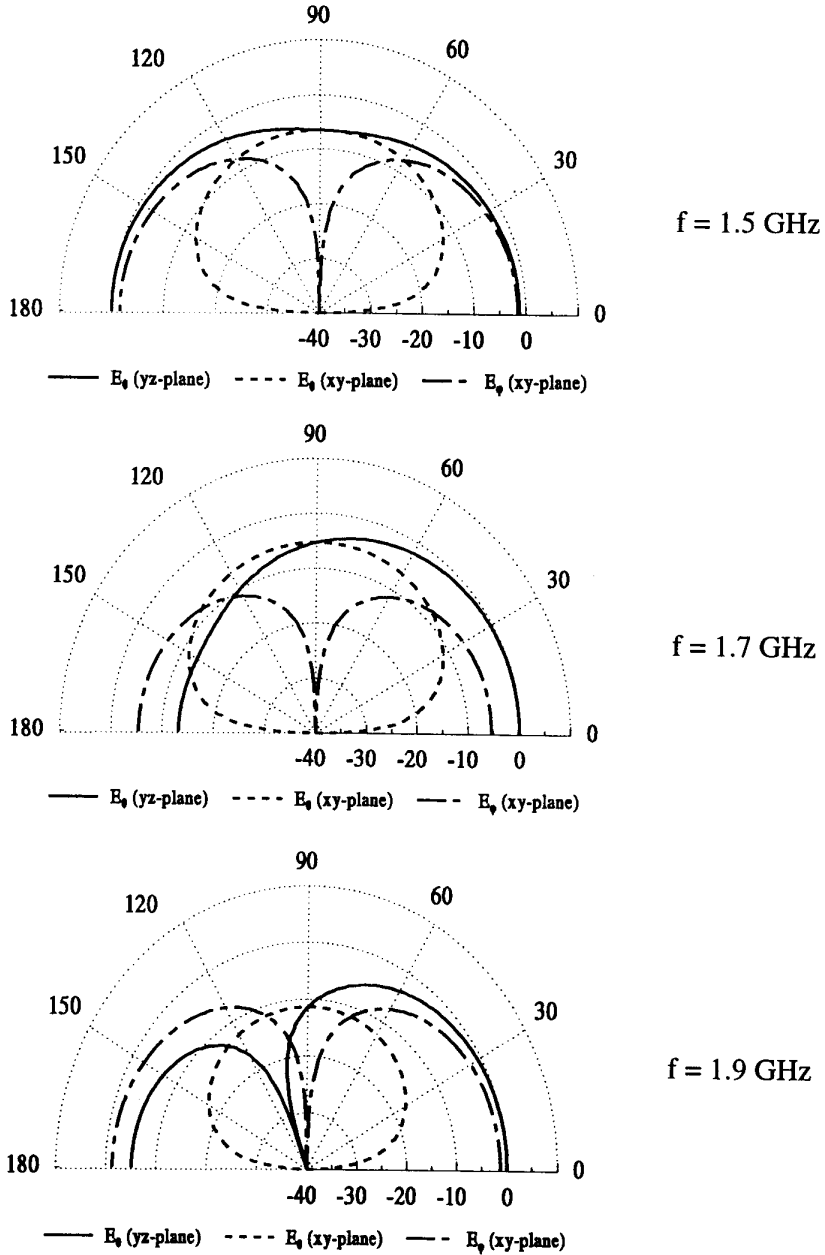


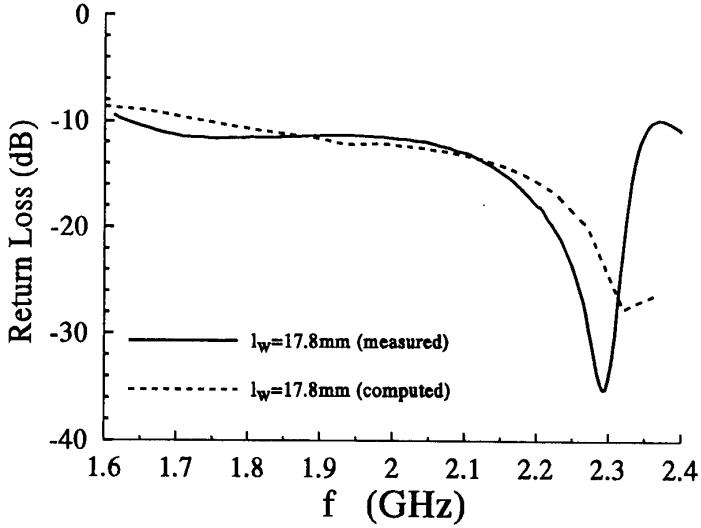
Figure 13. Return loss versus frequency with  $z_f = 3.95$  mm.

#### 4. DUAL-BAND ANTENNAS

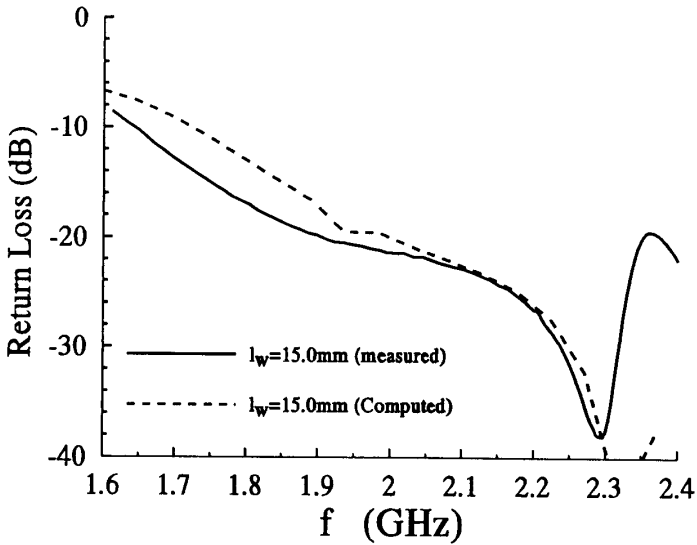
To obtain a dual-band antenna, we must excite either two different modes having similar far field patterns with the required frequency separation or have two resonators of different sizes and/or materials operating in the same mode but at a different frequency. The latter approach using two resonators will make the antenna larger in size. A different possible approach, however, is to combine the two resonators together as if one resonator is loading the other. In this case, the design process is more difficult and requires many trials to reach to the required characteristics. Here we present an example of a dielectric resonator with  $h_2 = 22.8$  mm,  $a_2 = 14.15$  mm, and  $\epsilon_2 = 36.0$  that is inserted inside a dielectric resonator with  $h_1 = 39.5$  mm,  $a_1 = 24.5$  mm, and  $\epsilon_1 = 12.0$ . The system is excited by a monopole located inside the smaller cylinder as illustrated in Fig. 17. The return loss of this antenna with different monopole lengths is shown in Fig. 18, where it can be seen that we have achieved multi-frequency operation. Figs. 19 and 20 show the radiation patterns at different frequencies and show that we have 3 different bands. The middle band is due to the excitation of the  $\text{HEM}_{12\delta}$  mode and the other two bands are influenced by the  $\text{HEM}_{11\delta}$  mode. The lower band appears to be due to the large DRA, while the upper band appears to be due to the smaller DRA.



**Figure 14.** Radiation patterns with  $z_f = 3.95 \text{ mm}$  and  $l_w = 15.75 \text{ mm}$ .



(a)



(b)

**Figure 15.** Return loss versus frequency with  $z_f = 0.0$  mm and (a)  $l_w = 17.8$  mm or (b)  $l_w = 15.0$  mm.

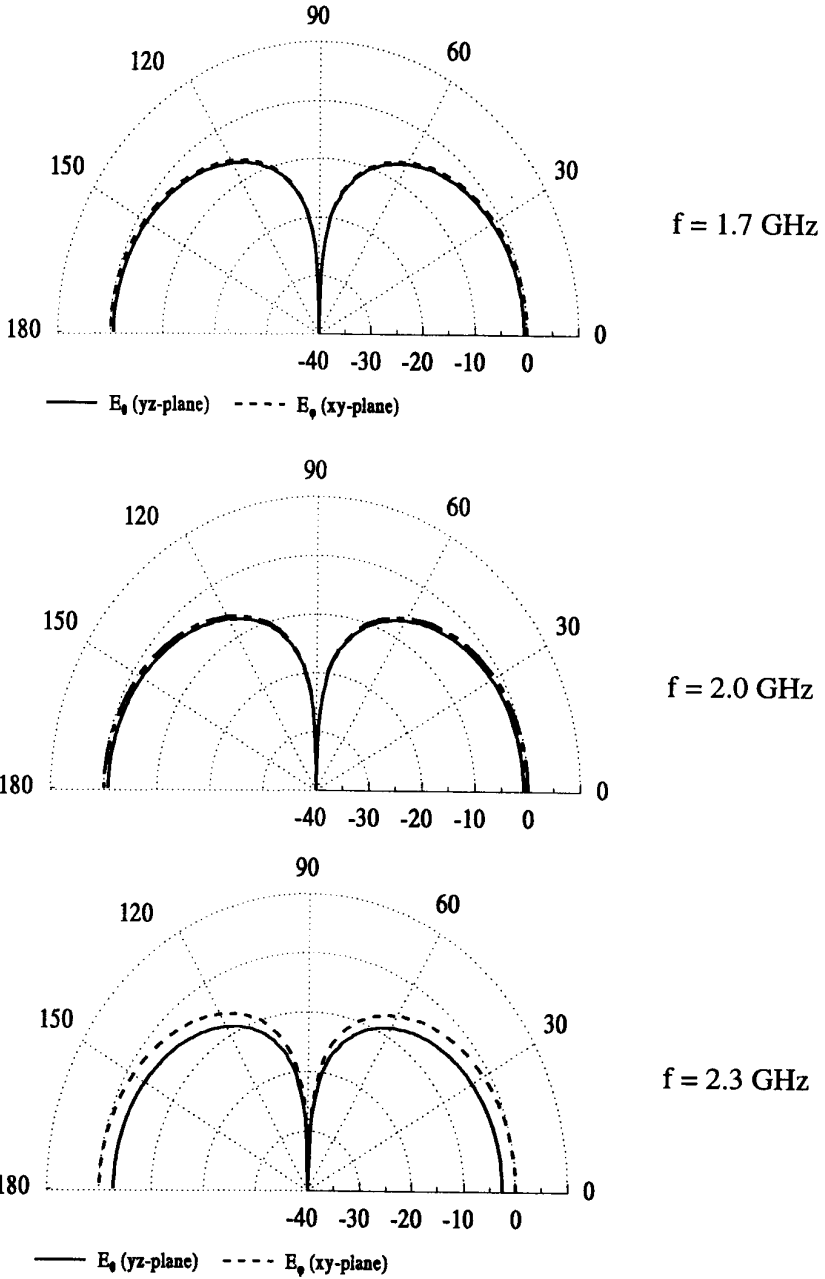
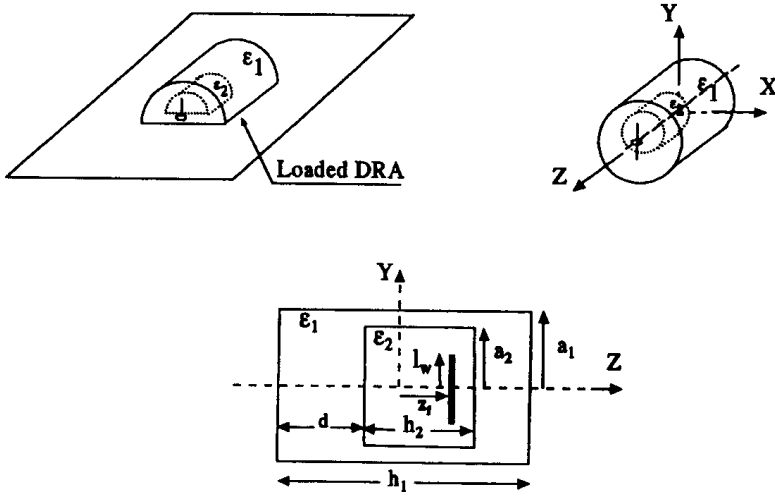
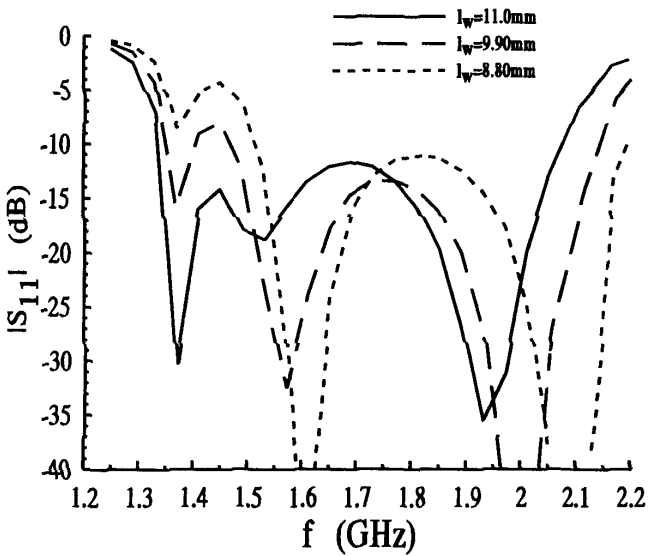


Figure 16. Radiation patterns with  $z_f = 0.0$  mm and  $\ell_w = 15.0$  mm.



**Figure 17.** Geometry for the loaded split DRA with vertical dipole located on the  $z$ -axis: 3-D and cross-section views.



**Figure 18.** Return loss versus frequency for the loaded split cylinder with the probe in the inner cylinder at  $z_f = 4$  mm.

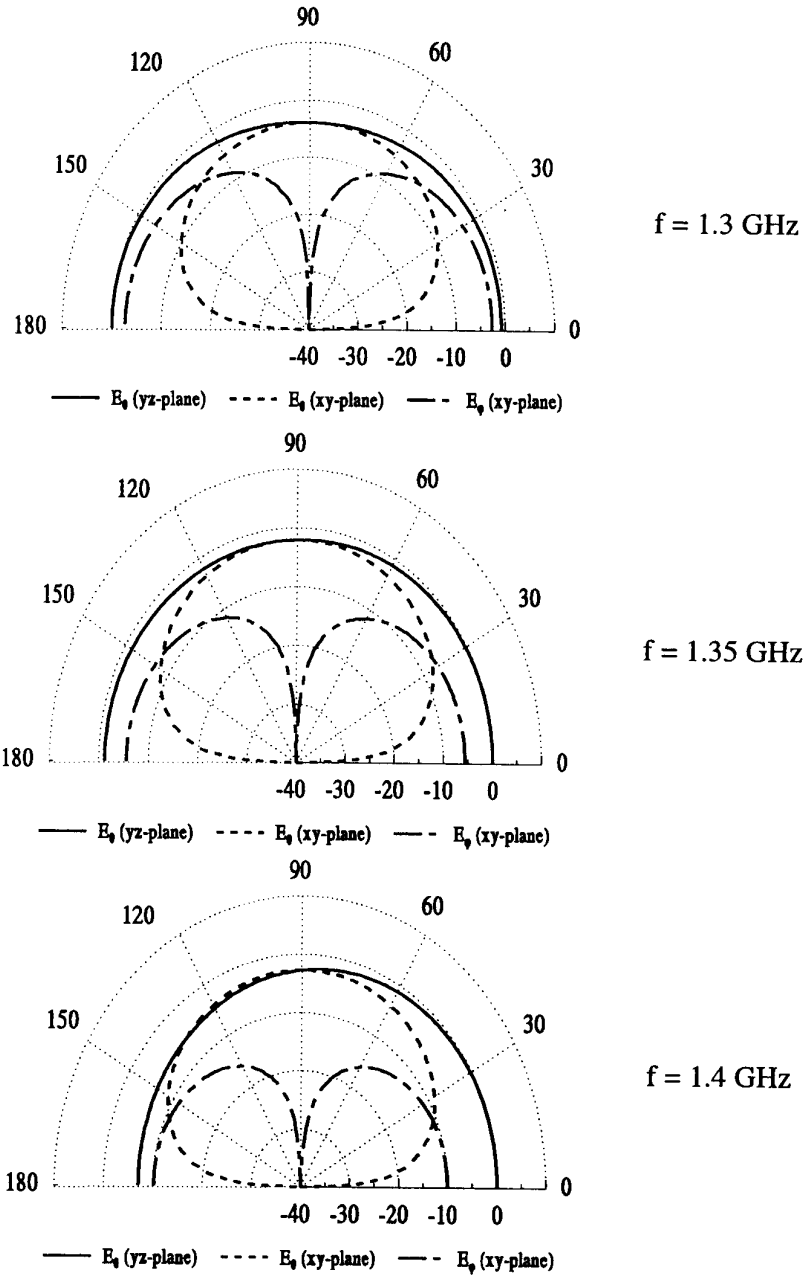


**Figure 19.** Radiation patterns for the loaded split DRA with  $z_f = 4 \text{ mm}$  and  $\ell_w = 11 \text{ mm}$  around  $f = 1.35 \text{ GHz}$ .

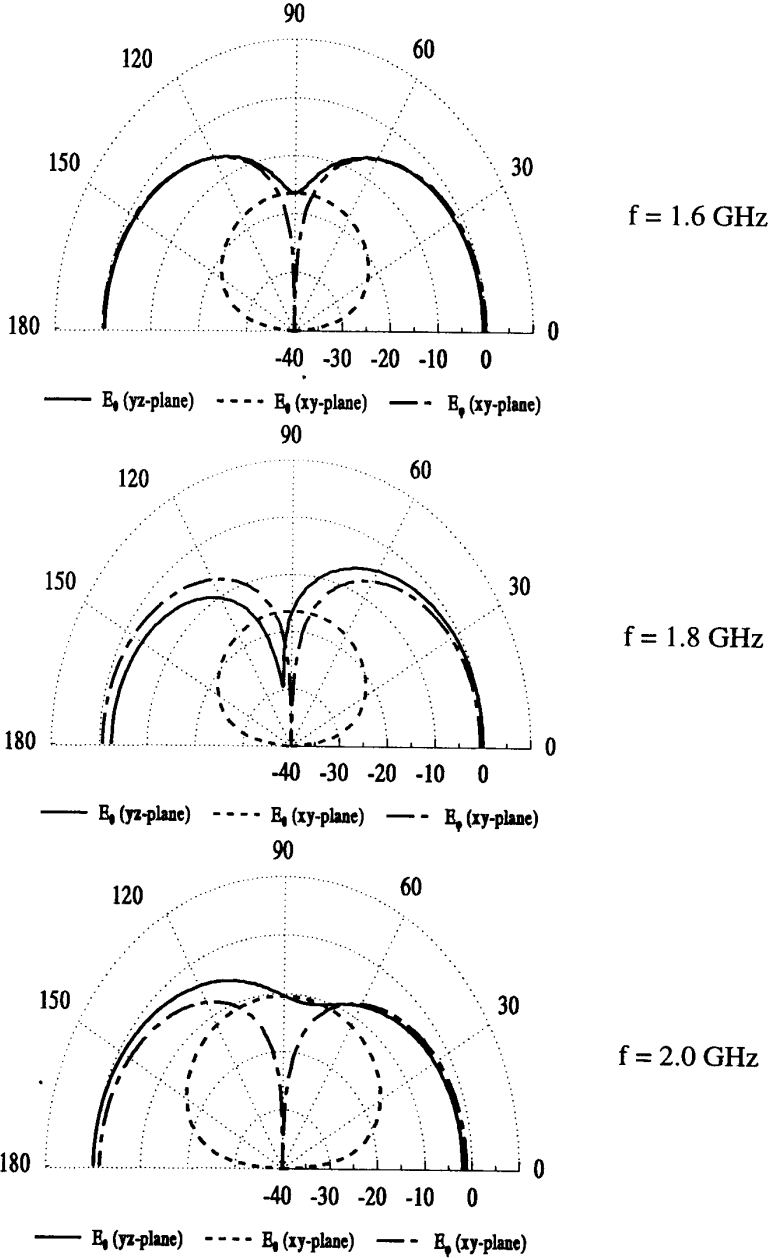


**Figure 20.** Radiation patterns for the loaded split DRA with  $z_f = 4$  mm and  $\ell_w = 11$  mm around  $f = 1.8$  GHz.

## 5. SUMMARY

In this paper we have presented a numerical study of two types of split cylindrical dielectric resonator antenna on a conducting ground plane excited by a coaxial probe. The numerical solution procedure is based on the method of moments for a body of revolution coupled to a wire. The split cylindrical dielectric resonator antennas considered in this study have been configured to operate primarily in either the  $HEM_{11}$  or  $HEM_{12}$  modes. By changing the parameters of the resonator and the excitation probe a wideband performance of about 35% has been achieved for some antenna configurations and experimental measurements have verified this performance. In addition, dual-band operation has been obtained by inserting a resonator of a different dielectric material inside another resonator.

## ACKNOWLEDGMENT

This work was partially supported by The Army Research Office under grant No. DAAG55-98-0308.

## REFERENCES

1. Kajfez, D. and P. Guillon (Ed.), *Dielectric Resonators*, Artech House, Norwood, MA, 1986.
2. Mongia, R. K., A. Ittipiboon, and M. Cuhaci, "Measurement of radiation efficiency of dielectric resonator antennas," *IEEE Microwave and Guided Wave Letters*, Vol. 4, No. 3, 80–82, 1994.
3. Junker, G. P., A. A. Kishk, and A. W. Glisson, "Input impedance of dielectric resonator antennas excited by a coaxial probe," *IEEE Trans. Antennas Propagat.*, Vol. AP-42, 960–966, July 1994.
4. Kishk, A. A., M. R. Zunoubi, and D. Kajfez, "A numerical study of a dielectric disk antenna above a grounded dielectric substrate," *IEEE Trans. Antennas Propagat.*, Vol. AP-41, 813–821, June 1993.
5. Junker, G. P., A. A. Kishk, and A. W. Glisson, "Input impedance of aperture coupled dielectric resonator antenna," *IEEE Trans. on Antennas and Propagation*, Vol. AP-44, No. 5, 600–607, May 1996.
6. Glisson, A. W., D. Kajfez, and J. James, "Evaluation of modes in dielectric resonators using a surface integral equation formulation," *IEEE Trans. Microwave Theory Tech.*, Vol. MTT-31, 1023–1029, December 1983.